CORA Cork Open Research Archive
Cartlann Taighde Oscailte Chorcaí

Title	Di-tert-butyl disulfide as a replacement for hydrogen sulfide in the atomic layer deposition of two-dimensional molybdenum disulfide
Authors	Campbell, Ian E.;Gupta, Aashi;Metaxa, Pavlina;Arifutzzaman, A.;Ma, Tao;Arellano, Paula;Duffy, Ray;Bol, Ageeth A.
Publication date	2025-02-11
Original Citation	Campbell, I. E., Gupta, A., Metaxa, P., Arifutzzaman, A., Ma, T., Arellano, P., Duffy, R. and Bol, A. A. (2025) 'Di-tert-butyl disulfide as a replacement for hydrogen sulfide in the atomic layer deposition of two-dimensional molybdenum disulfide', Chemistry of Materials, 37(4), pp.1478-1490. https://doi.org/10.1021/acs.chemmater.4c02561
Type of publication	Article (peer-reviewed)
Link to publisher's version	10.1021/acs.chemmater.4c02561
Rights	© 2025, American Chemical Society. This document is the Accepted Manuscript version of a Published Work that appeared in final form in Chemistry of Materials after technical editing by the publisher. To access the final edited and published work see: https://doi.org/10.1021/acs.chemmater.4c02561
Download date	2026-11-05 22:19:36
Item downloaded from	https://hdl.handle.net/10468/17062

UCC
University College Cork, Ireland
Coláiste na hOllscoile Corcaigh

Di-tert-butyl Disulfide as a Replacement for Hydrogen Sulfide in the Atomic Layer Deposition of Two-Dimensional Molybdenum Disulfide

Ian E. Campbell,[1] Aashi Gupta,[2] Pavlina Metaxa,[2] A. Arifutzzaman,[2] Tao Ma,[1] Paula Arellano,[1] Ray Duffy[2], Ageeth A. Bol[1]

[1] The University of Michigan, Ann Arbor, Michigan, 48109, United States of America.

[2] Tyndall National Institute, University College Cork, Lee Maltings, Cork T12 R5CP, Ireland.

SUPPORTING INFORMATION

SUMMARY OF THE TWO-STEP H_2S-BASED ALD PROCESS

The H_2S plasma- based ALD process is schematically outlined in Figure S1. Note that the first purge is divided into a 3 s rough pumping step immediately following the precursor dose, then a 9 s turbo pumping step, and then the co-reactant gas flow rates are stabilized for 3 seconds before striking the plasma. The second purge begins with a 3 s gas stabilization step to remove excess H_2S and H_2 from the space between the MFC and pneumatic valve upstream to limit the potential for the leaking of process gases through MFCs during the metalorganic dose. The second and third steps of the second purge are a 6 s pump down using the turbo pump, followed by a 6 s pump down using the rough pump. These times were chosen to allow the chamber pressure to equilibrate before beginning the next dose. The carrier gas flow (Ar) was set to 30 sccm and the ellipsometer purge and transfer gate purge valves were set to flow rates of ~25 sccm of Ar for the entire recipe. The plasma gas flow was set to 80 sccm of Ar for the metalorganic dosing step.

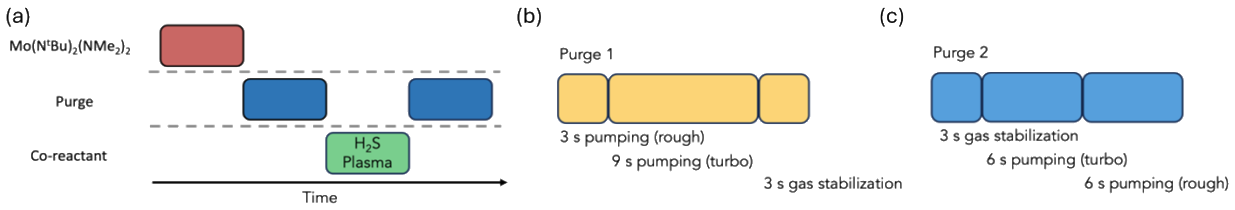


Figure S1. (a) Schematic depicting the two-step ALD process using $(tBuN)_2(NMe_2)_2Mo$ as a Mo precursor and H_2S as a sulfur precursor. (b) Schematic showing the structure of the first purge in the two-step H_2S-based ALD process. (c) Schematic showing the structure of the second purge in the two-step H_2S-based ALD process.

PROCESS DEVELOPMENT FOR THE H_2S AND TBDS-BASED PROCESSES

Saturation times for the H_2S-plasma process were measured at a deposition temperature of 350 °C, while recording apparent film thickness values every 0.5s via iSE. The $(tBuN)_2(NMe_2)_2Mo$ saturation curve shown in Figure S2a was collected from a recipe using a 60 s $(tBuN)_2(NMe_2)_2Mo$ dose and a 10 s $H_2S/H_2/Ar$ (2 sccm/8 sccm/40 sccm) plasma dose. A $(tBuN)_2(NMe_2)_2Mo$ dose time of 15 seconds was chosen to balance maximizing the saturating ALD behavior with minimizing the linear, CVD-like behavior. The $H_2S/H_2/Ar$ plasma saturation curve shown in in Figure S2b below was collected using a 15 s $(tBuN)_2(NMe_2)_2Mo$ dose and a 30 s plasma dose. A dose time of 10 s was chosen for the $H_2S/H_2/Ar$ plasma since the ALD-related term of the model appears saturated at that time and there is a minimal contribution from the linear term for all times.

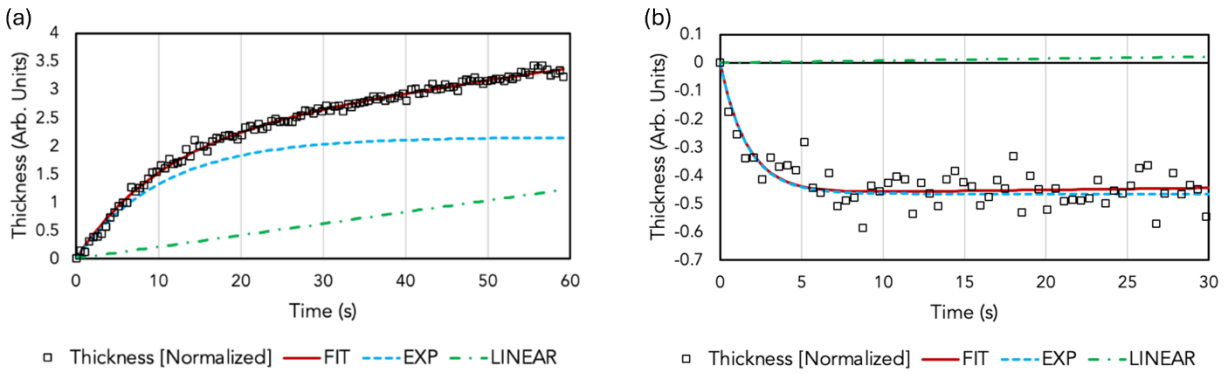


Figure S2. Saturation curves for the $(tBuN)_2(NMe_2)_2Mo$ dose (a) and the H_2S plasma dose (b) from the two-step H_2S-based ALD process collected via in-situ spectroscopic ellipsometry.

Real-time iSE data was acquired in 2 s increments during the growth of two films using 100 ALD cycles of the TBDS and H_2S-based processes. The thickness data acquired from these depositions were fit via linear regression. These thicknesses and the slope of the

linear model were used to evaluate the growth rates of each ALD process. All thickness values were obtained from iSE data modeled in CompleteEASE using a model composed of a B-spline layer on top of an SiO_2 layer.

RGA measurements acquired from a stop-flow version of the TBDS-based ALD process show cyclic changes in the prevalence of species with M/Z = 2 and 40 (Figure S 3), which likely result from the singly charged process gases Ar and H_2. Note that the signal for H_2 spikes only during the H_2 plasma dose and the Ar signal spikes for each ALD step since Ar is used continually as a carrier gas, causing the process chamber pressure to spike during stop-flow doses. The dips in the H_2 signal seem to correlate with increased Ar signal, perhaps indicating that Ar flowing from the increasingly pressurized process chamber helps to lower the concentration of H_2 in the mass spectrometer. Similar dips in intensity are observed for species with M/Z = 16, 17, and 18, however, there is also a recurring spike for these species during the H_2 plasma exposure. The presence of species with M/Z = 16, 17, and 18 theoretically indicates the presence of methane, ammonia, and water respectively. Thus, it appears these signatures could be considered a collection of signals from methane, ammonia, and water derived from the reaction between the H_2 plasma and oxygen contamination (resulting in water) and Mo precursor ligands adsorbed to the

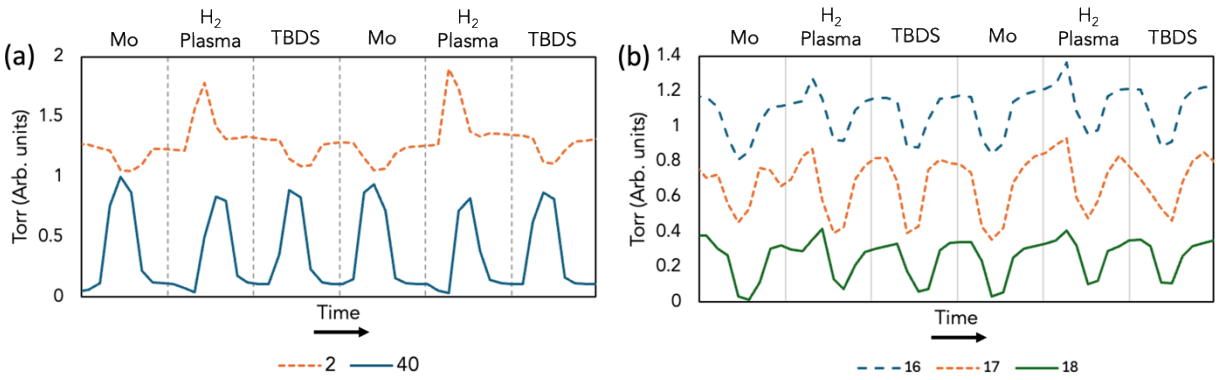


Figure S 3. Intensity normalized RGA measurements taken from the TBDS-based ALD process for species with M/Z = 2 and 40 (a) and M/Z = 16, 17, and 18 (b).

surface in the previous ALD step (resulting in methane and ammonia). However, the fragmentation of water into -OH (M/Z = 17) and -H and ammonia into -NH_2 (M/Z = 16) and H due to ionization within the mass spectrometer could obfuscate the true nature of these signals.

GPC values were determined across a range of deposition temperatures by depositing MoS_2 using 100 cycles of the TBDS and H_2S processes, then characterizing the resulting films' thicknesses using ex-situ spectroscopic ellipsometry (Figure S4). Note the presence of a plateau in growth rate at ~ 300-400 °C for each process.

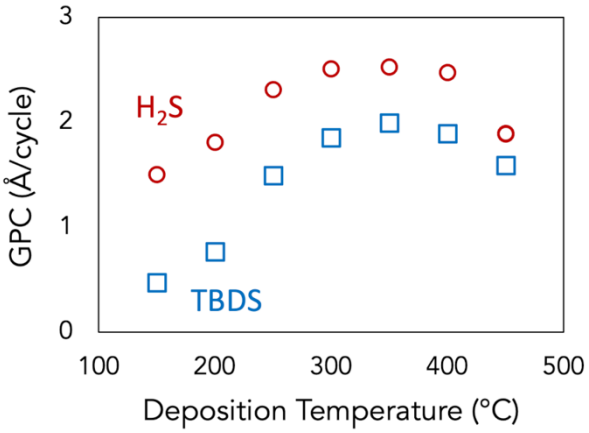


Figure S4. Growth-per-cycle (GPC) recorded for the H_2S and TBDS-based ALD processes. Each GPC was found by measuring the total MoS_2 thickness deposited using 100 cycles of each process at deposition temperatures ranging from 150 to 450 °C.

STEP-HEIGHT MEASUREMENT VIA AFM FOR GPC MEASUREMENTS

AFM analysis was performed on two films made with 100 cycles of each ALD recipe to measure the films' thicknesses. Each film was scratched and measured via AFM to determine the step height of the scratch. Note that the film synthesized with the H_2S-based ALD process shown in the AFM image below (Figure S5a) is only present on the left side of the image and the scratch where no film is present is the dark area on the right side of the image. The corresponding plot (Figure S5b) show profiles of the step as determined by vertically averaging the associated AFM image. A similar analysis was performed for a film made with the TBDS-based ALD process as shown by the AFM image (Figure S5c) and step profile (Figure S5d). The step profiles indicate

that the film thicknesses are 15 and 11 nm for the films made with H_2S and TBDS, respectively, meaning that the growth per cycle (GPC) values are 1.5 and 1.1 Å/cycle.

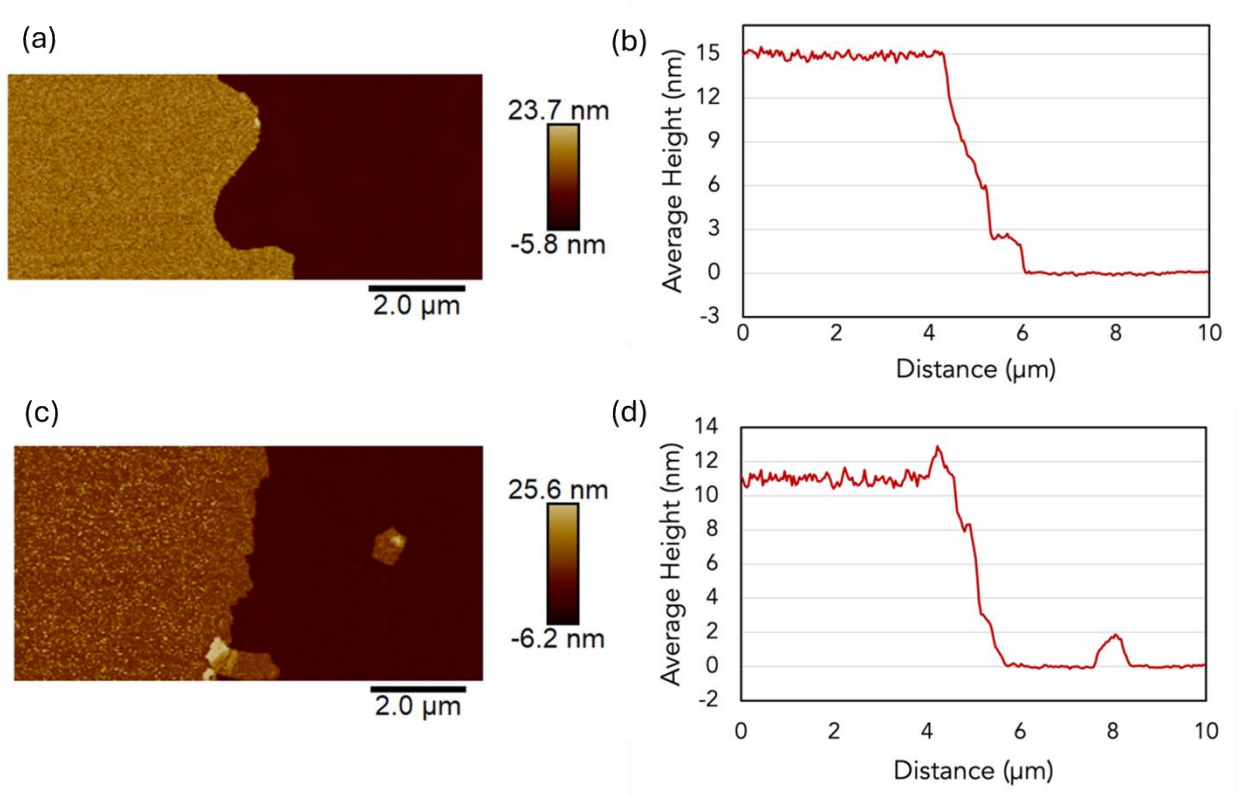


Figure S5. AFM image (a) and associated height profile (b) for a MoS_2 film made with 100 cycles of the H_2S-based ALD process. AFM image (c), and associated height profile (d) for a MoS_2 film made with 100 cycles of the TBDS-based ALD process. The height profiles are constructed by vertically averaging the respective AFM images.

RAMAN ANALYSIS

Raman spectroscopy shows the E^1_{2g} and A_{1g} peaks characteristic of MoS_2 for films synthesized at all deposition temperatures ranging from 150 to 450 °C (Figure S6). The H_2S process is capable of synthesizing MoS_2 at lower deposition temperatures compared to the TBDS-based process.

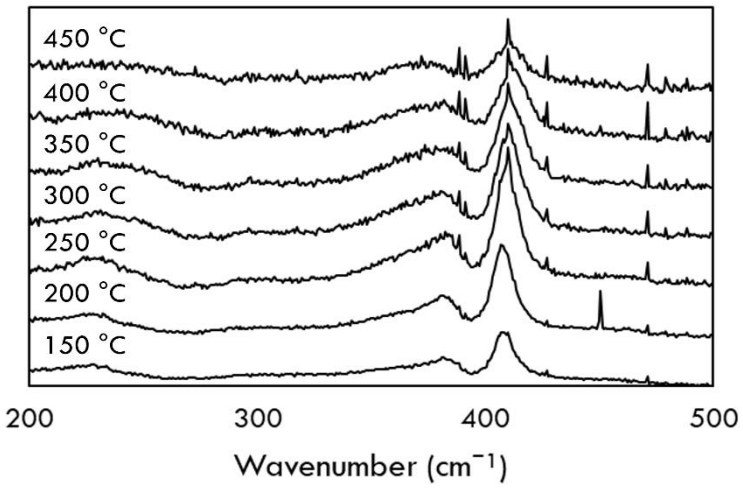


Figure S6. Raman spectra acquired from MoS_2 films made with 100 cycles of the H_2S-based ALD process at deposition temperatures ranging from 150 to 450 °C. Each spectrum is normalized to the maximum of the Si substrate signal at 520.6 cm^{-1}.

Raman peak positions, their full-widths at half their maximum intensity (FWHM), and their areas are reported in Table S **1** with corresponding errors as calculated in Origin. Note there are large errors associated with the defect-related modes, thus we have refrained from intensively analyzing defect type and instead focus on the relative intensity of these modes between the two ALD processes.

Table S 1. Tabulated data for two ~10 nm films made using the H_2S and TBDS-based ALD processes.

	$H_2S/H_2/Ar$ plasma			H_2 plasma + TBDS		
Raman Mode	Position (cm^{-1})	FWHM (cm^{-1})	Area (arb. Units)	Position (cm^{-1})	FWHM (cm^{-1})	Area (arb. Units)
TO(M)	358 ± 8	25 ± 10	0.4 ± 0.3	362 ± 45	36 ± 43	0.87 ± 4
LO(M)	375 ± 5	18 ± 12	0.4 ± 0.6	374 ± 20	16 ± 52	0.31 ± 5
E^1_{2g}	383.8 ± 0.7	10 ± 2	0.3 ± 0.3	382 ± 3	9 ± 7	0.14 ± 0.5

A_{1g}	408 ± 1	10 ± 2	1.3 ± 1	407 ± 2	11 ± 3	1.03 ± 1
ZO(M)	413 ± 12	13 ± 3	0.4 ± 1	413 ± 9	12 ± 4	0.42 ± 0.9

XPS ANALYSIS OF A MOS_2 FILM SYNTHESIZED USING H_2S

All peaks were fit with a numerical convolution of Gaussian and Lorentzian line shapes denoted as the 'LA' line shape in CasaXPS. A symmetric LA(50) line shape was used to fit the Mo3d and S2p peaks, a symmetric LA(90) line shape was used to fit the S2s peak, an asymmetric LA(1, 3, 50) line shape was used to fit the C1s peak, and a symmetric LA(1.5, 1.5, 10) line shape was used to fit the Mo 3p and N 1s peaks. Peak areas were adjusted using their respective relative sensitivity factors prior to drawing conclusions about film stoichiometry. All XPS data were fit using an 'Iterated Shirley' type background with endpoints having an intensity equal to the average intensity for the last five data points at either end of each data set.

The same XPS spectra that were collected for MoS_2 films made with TBDS were collected for films made with H_2S and are shown in Figure S7. The Mo 3d region (Figure S7a) acquired from the film made with H_2S is indicative of MoS_2 and is highly similar to the Mo 3d region acquired from the film made with TBDS. The S 2p (Figure S7b) and N 1s regions (Figure S7c) observed for MoS_2 made with H_2S are also similar to those collected for MoS_2 made with TBDS, except the peak associated with the N 1s signal is slightly more intense in the data acquired from MoS_2 made with H_2S. The plot in Figure S7d depicting the ratio of the C 1s signal area to the Mo 3d signal area for various collection angles also resembles the analogous dataset acquired for the film made with TBDS. Overall, the two processes appear to synthesize MoS_2 with similar composition.

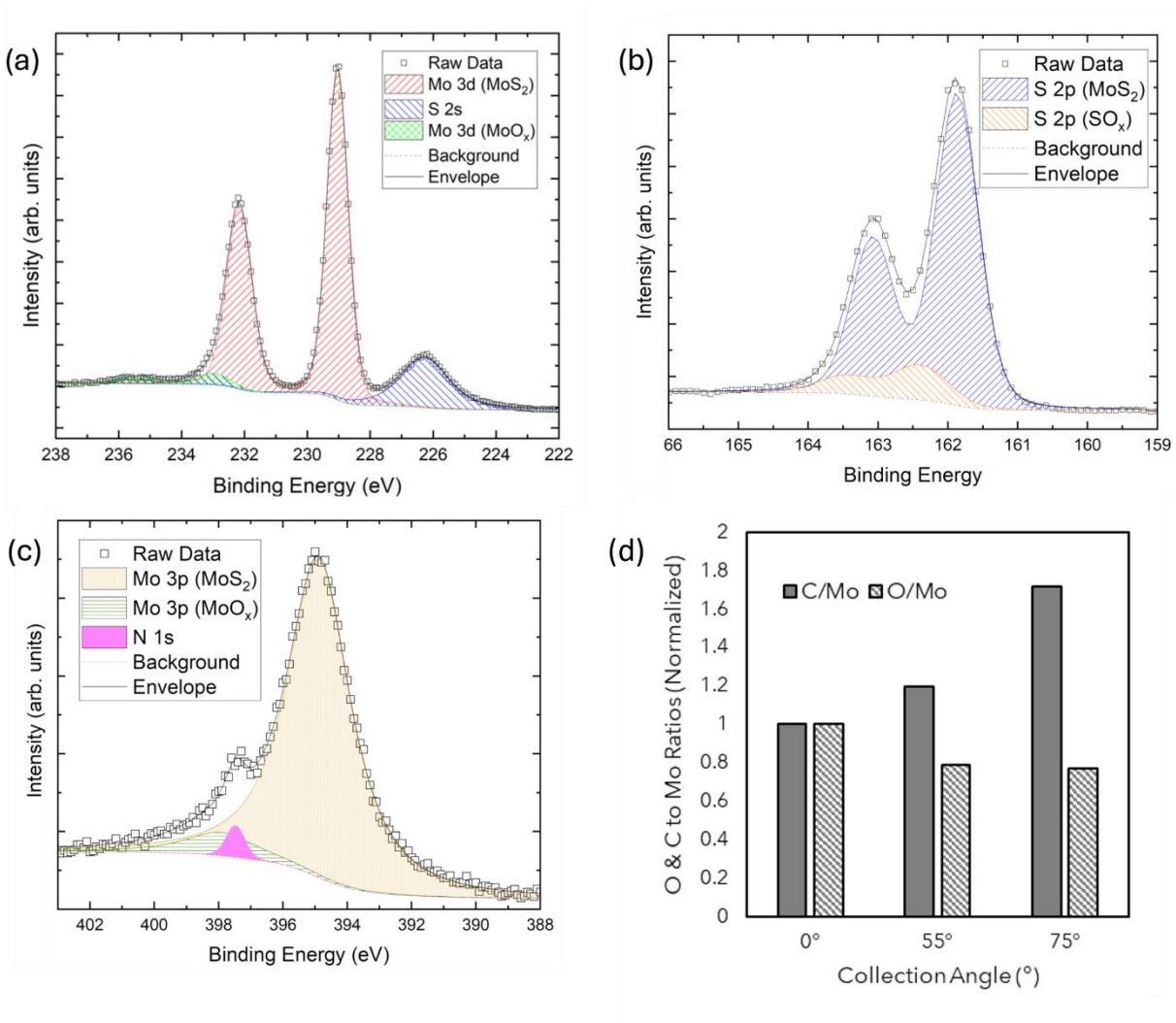


Figure S7. XPS data acquired from a ~10 nm thick MoS_2 film made with the three-step H_2S-based process. (a) Fitted XPS spectrum of the Mo3d and S 2s regions. (b) Fitted XPS spectrum of the S 2p region. (c) Fitted XPS spectrum of the Mo 3p 5/2 and N 1s regions. (d) Relative areas of peaks fit to XPS spectra featuring the C 1s and O 1s regions. The C 1s and O 1s regions were normalized for each film so that the peak areas for spectra collected at an angle of 0° are equal to 1 relative to the corresponding Mo 3d signal.

CROSS-SECTIONAL TEM ANALYSIS

Sample cross sections (lamellae) for analysis using cross-sectional TEM were prepared employing a Dual Beam focused ion beam (FIB) system, specifically the FEI Helios NanoLab 600i. Prior to FIB milling, electron beam-induced deposition was used to deposit carbon layers ranging from 50 to 100 nm in thickness, platinum layers ranging from 50 to 150 nm, and, finally, 3.5 μm thick carbon layers on each sample. The prepared lamellae were then lifted out and positioned onto a molybdenum sample grid (Ted Pella, Inc.). Lamellae were further thinned at 30

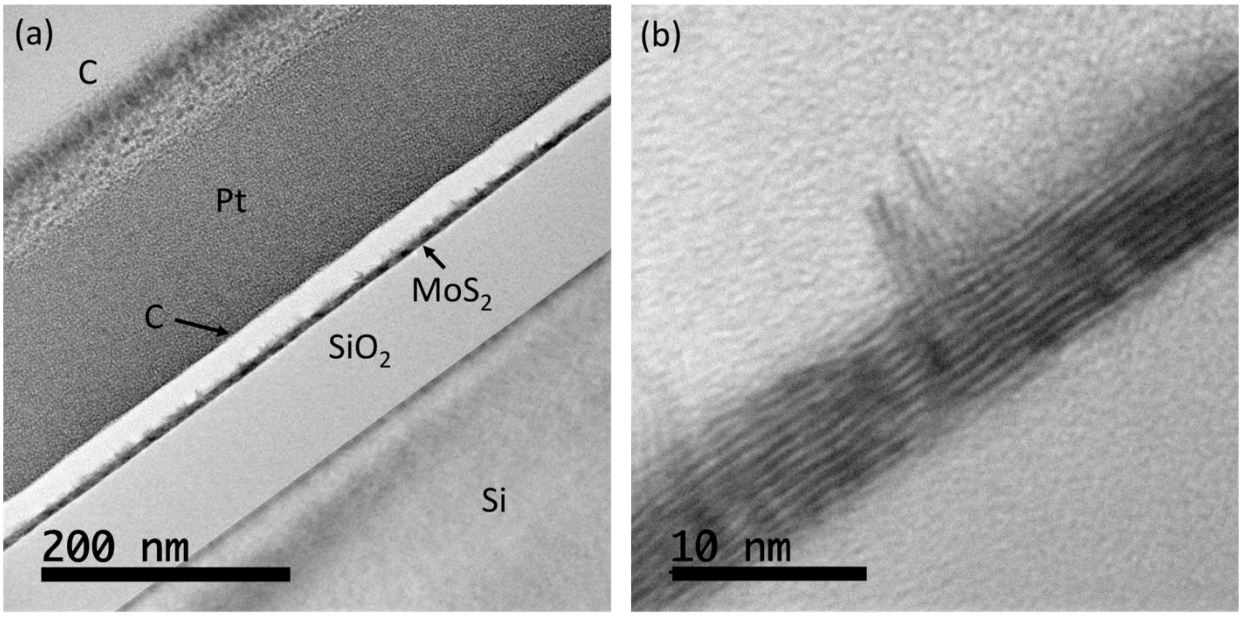


Figure S8. (a) Zoomed-out cross sectional view of a ~10 nm thick MoS_2 film deposited using H_2S on a 90 nm SiO_2 layer on a Si wafer. (b) Magnified view of a ~10 nm thick MoS_2 film. The protective carbon and platinum layers are visible in the zoomed-out micrograph.

kV (0.28 nA), followed by a final polish at 5 kV (47 pA) to minimize FIB ion-beam-induced damage.

Cross-sectional TEM was used to evaluate the appearance of each MoS_2 film and to determine whether a layered van der Waals structure had been synthesized. Figure S8a depicts the cross section cut from a ~10 nm thick MoS_2 film deposited on an SiO_2/Si substrate using H_2S as a sulfur precursor. Figure S8b shows the same cross section at a higher magnification. Note the presence of light and dark striations the bulk of which are parallel to the substrate, but some of which are perpendicular to the substrate. The striations are indicative of MoS_2 layers alternating with van der Waals gaps. Those parallel to the substrate are called "in-plane" growth while those perpendicular to the substrate are "out-of-plane" growth or fins. These findings are similar to those observed via cross-sectional TEM for the MoS_2 film made with TBDS as both films are predominantly in-plane with some out-of-plane fins.

PLAN-VIEW TEM ANALYSIS OF MOS_2 FILMS

TEM grids contained one 0.25 x 0.25 mm 10 nm thick silicon nitride window (Norcada). Prior to the deposition of MoS_2, each TEM grid was coated with SiO_2 via ALD at 200 °C in preparation of their use as substrates for MoS_2 ALD. The SiO_2 ALD process had a growth per cycle of 0.735 Å / cycle, so 68 cycles were performed to deposit a layer ~5nm thick. Bis(diethylamino)silane (60 ms dose time) was used as a Si precursor and an O_2 plasma (20 s dose time, 50 sccm O_2, 100 sccm Ar, 300 W) was used as the oxygen precursor.

Plan-view HAADF STEM was used to characterize the microstructure of a ~5 nm thick MoS_2 film made with H_2S. Figure S **9**a depicts a plan-view HAADF STEM micrograph of the ~5nm MoS_2 film. Lighter regions in this image correspond with thicker portions of the film, specifically portions of the film where out-of-plane growth has occurred, while darker regions of this micrograph correspond to the portions of the film where in-plane growth has occurred. The inset of Figure S **9**a depicts an FFT constructed from the plan-view HAADF STEM micrograph using ImageJ software. The ring in this FFT (highlighted by a blue arc) corresponds to a

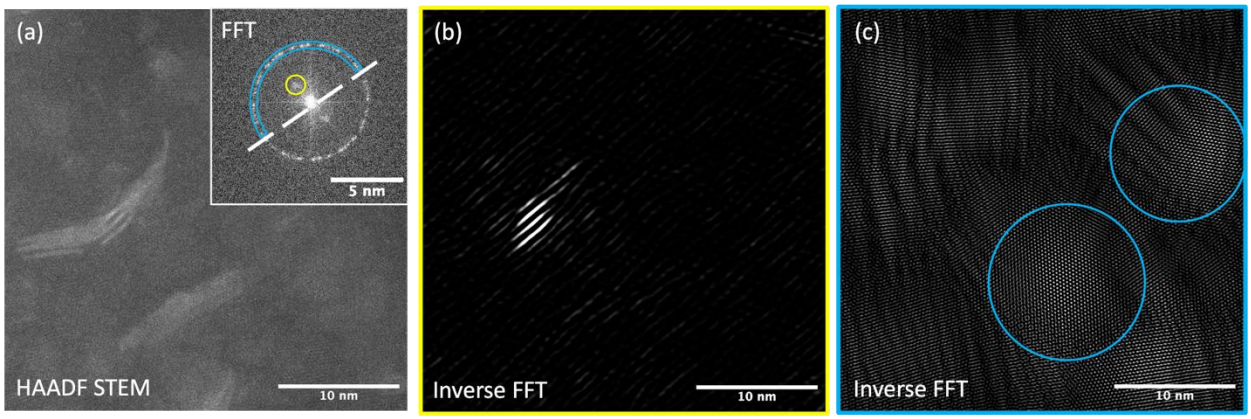


Figure S 9. Plan-view HAADF-STEM image depicting a 5 nm thick MoS_2 film deposited using TBDS on a 10 nm thick silicon nitride TEM window membrane previously coated with 5 nm of atomic layer deposited SiO_2; the inset depicts the corresponding FFT (a). An inverse FFT (b) constructed from the spot contained in the yellow circle in the inset in (a), note the presence of lattice fringes consistent with interlayer spacing in MoS_2 (b). An inverse FFT (c) constructed from the spots contained in the blue arc in the inset in (a), note the lighter regions ~10 nm in diameter, some of which are indicated by circles.

crystallographic spacing of ~0.27 nm, while the spot (highlighted by a yellow circle) corresponds to a spacing of 0.61-0.70 nm. Inverse FFTs were constructed from the ring and the spot in the FFT to highlight areas of the film possessing features with the corresponding periodicity. Figure S **9**b is an inverse FFT constructed from the spot highlighted in yellow and clearly highlights an out-of-plane fin possessing a layered structure indicative of MoS_2. Figure S **9**c is an inverse FFT

constructed from the ring highlighted in the blue arc and shows bright regions approximately 10 nm in diameter that correspond with regions of greater crystallographic order (i.e. crystal grains). The crystal grains viewed this way in the MoS_2 film made with H_2S appear to be similar in size to those observed for the film made with TBDS.

Constructing an inverse FFT, like those in Figure S **9**b and **c**, from a ring in an FFT, like that in the inset of Figure S **9**a, simultaneously yields information from multiple crystal grains having many orientations. Constructing inverse FFTs from individual spots in the ring should theoretically highlight crystal grains of one orientation. Figure S10a and b and Figure S11a and b are the plan-view HAADF STEM micrographs and FFTs shown in Figure S **9**a and Figure S11a, respectively. Note that the rings in the FFTs shown in Figure S10b and Figure S11b are composed of individual spots. Five of these spots were isolated for both plan-view HAADF STEM micrographs and used to construct inverse FFTs via ImageJ software to aid in the determination of the crystal grain size in each film. Figure S10c-g and Figure S11c-g are inverse FFTs with inset FFTs annotated with a blue circle indicating the spot that was isolated and used to construct the associated inverse FFT. Note the presence of lighter regions roughly 10 nm across in each inverse FFT.

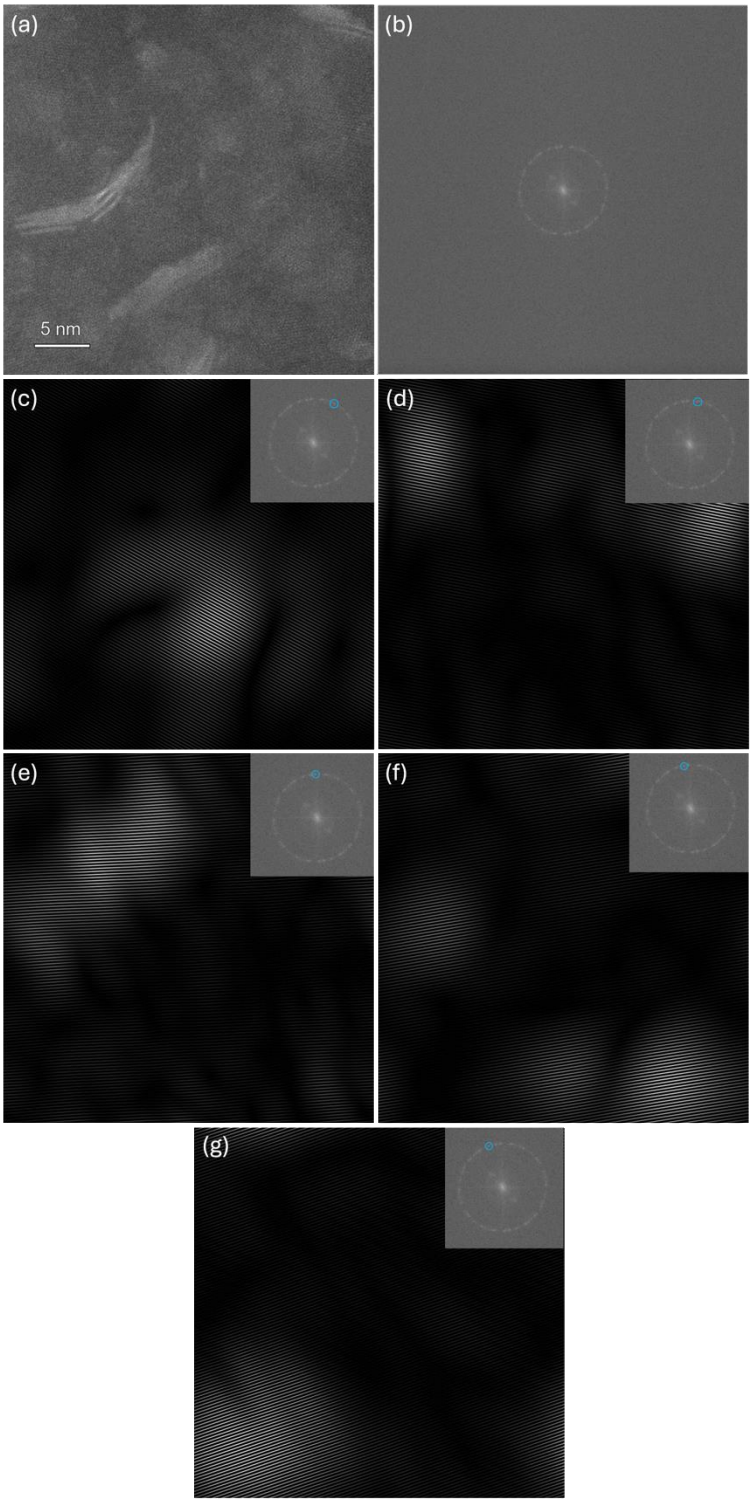


Figure S10. HAADF-STEM image of a 5 nm MoS2 film made with H_2S (a), associated FFT (b), and five pairs of inverse FFTs (c-g) and FFTs (insets) showing which spots have been used to construct the associated inverse FFTs.

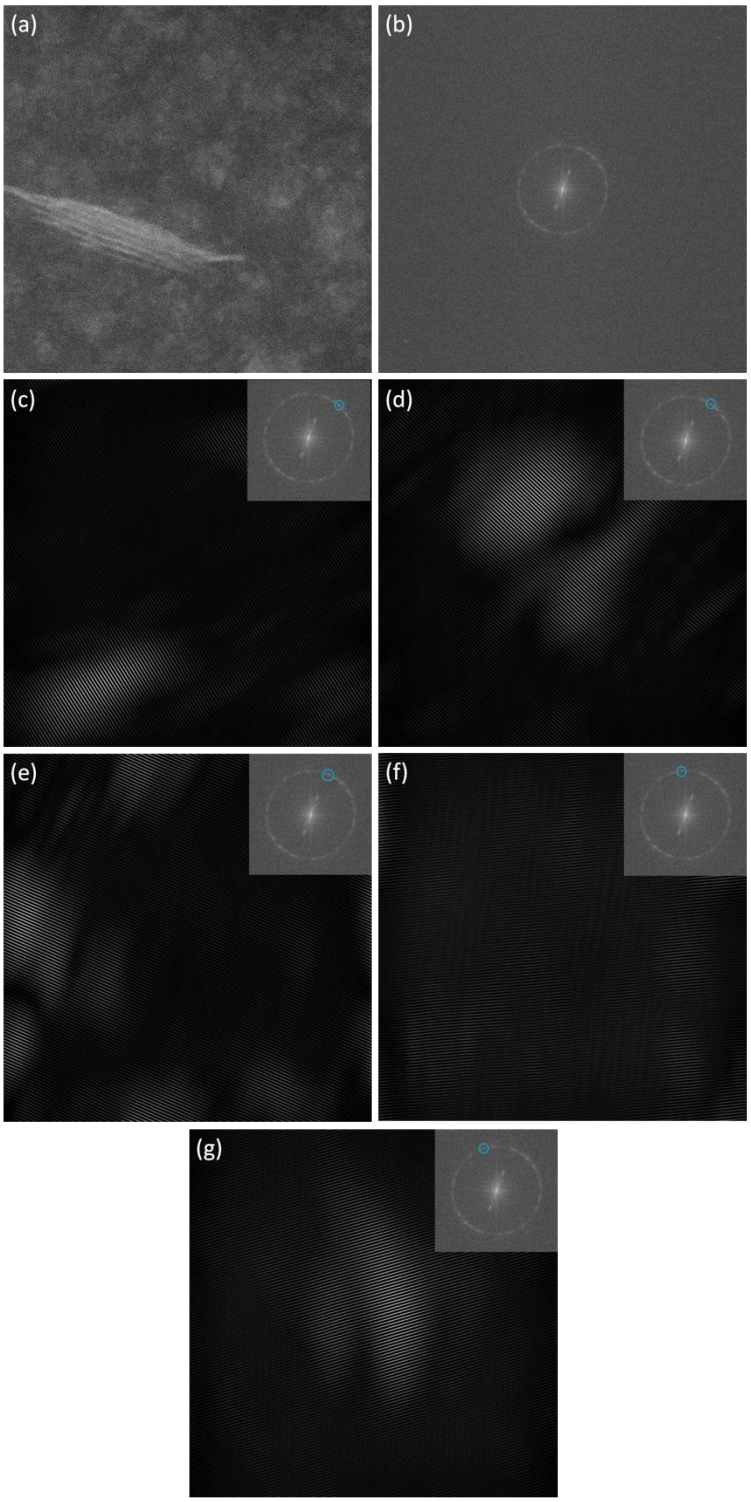


Figure S11. HAADF-STEM image of a 5 nm MoS_2 film made with TBDS (a), associated FFT (b), and five pairs of inverse FFTs (c-g) and FFTs (insets) showing which spots have been used to construct the associated inverse FFTs.

Three more HAADF-STEM images were taken from films made with the TBDS (Figure S12) and H_2S (Figure S13) process and were analyzed by constructing FFTs and then inverse FFTs to highlight regions in the original images associated with the $\{1\bar{1}00\}$ planes as was done for the images in Figure 10 and Figure S 9.

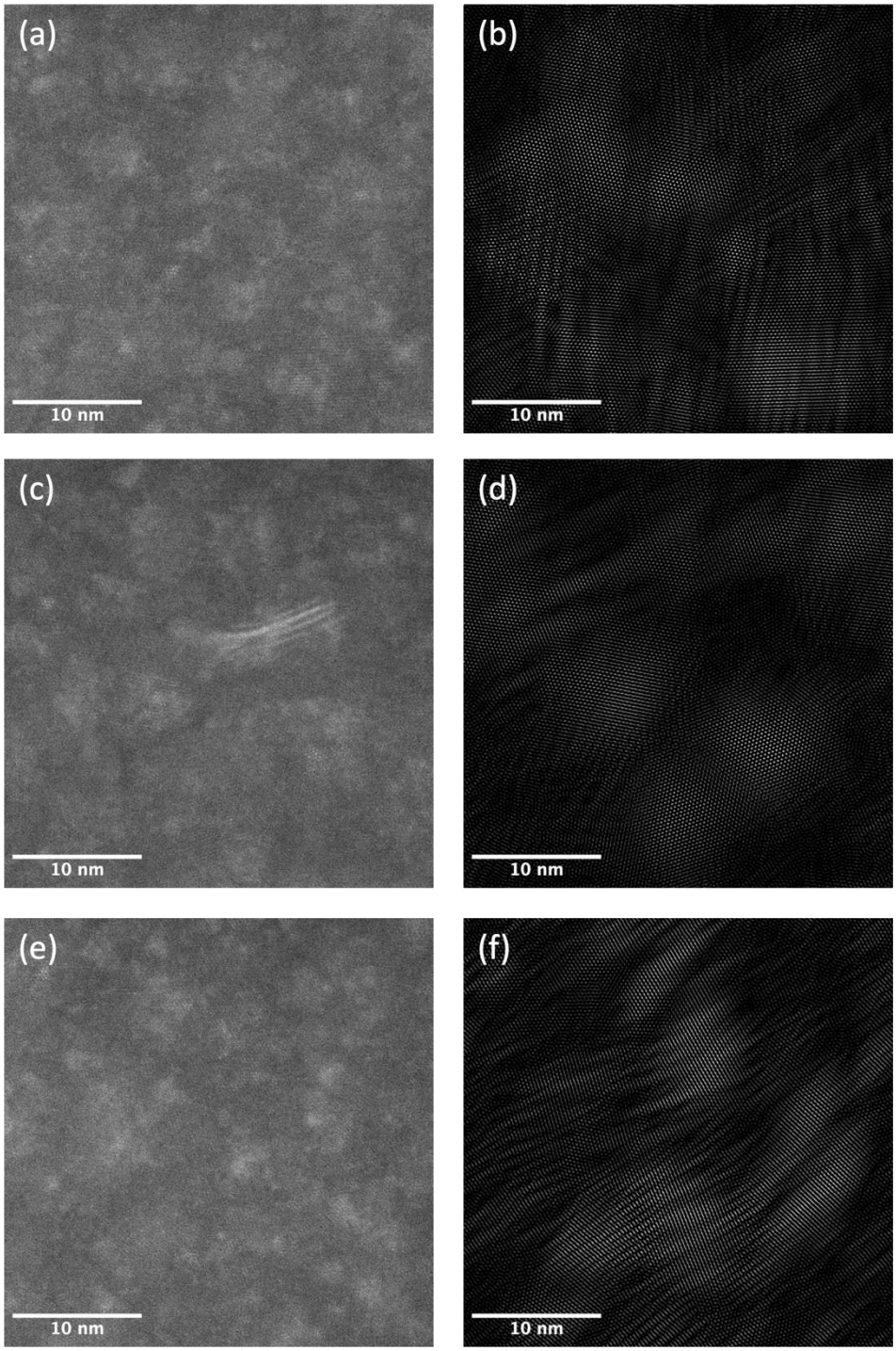


Figure S12. Plan-view TEM micrographs collected from multiple locations on a ~5nm thick MoS_2 film made using TBDS and their associated inverse FFTs showing crystallographically ordered regions (light regions) roughly ~10 nm in size.

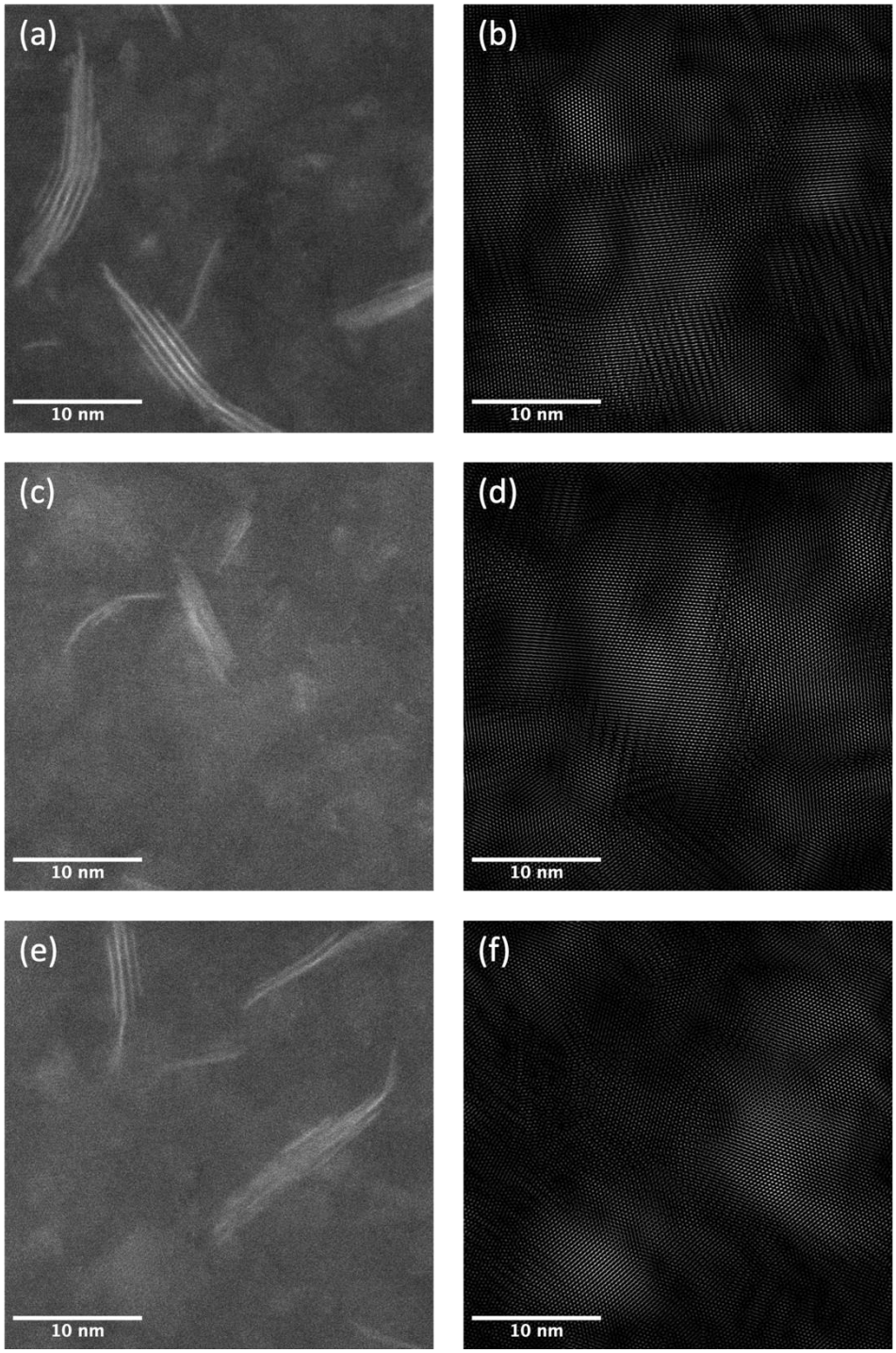


Figure S13. Plan-view TEM micrographs collected from multiple locations on a ~5nm thick MoS_2 film made using H_2S and their associated inverse FFTs showing crystallographically ordered regions (light regions) roughly ~10 nm in size.